Exploring Self-Repair in a Coupled Spiking Astrocyte Neural Network

Junxiu Liu, *Member, IEEE,* Liam J. McDaid, Jim Harkin, *Member, IEEE,* Shvan Karim, Anju P. Johnson, *Member, IEEE,* Alan G. Millard, *Member, IEEE,* James Hilder, David M. Halliday, Andy M. Tyrrell, *Senior Member, IEEE,* and Jon Timmis, *Senior Member, IEEE*

***Abstract*—It is now known that astrocytes modulate activity at tripartite synapses where indirect signalling via the retrograde messengers, endocannabinoids, leads to a localised self-repairing capability. In this paper, a self-repairing Spiking Astrocyte Neural Network (SANN) is proposed to demonstrate a distributed self-repairing capability at the network level. The SANN uses a novel learning rule which combines the spike timing dependent plasticity (STDP) and Bienenstock, Cooper, and Munro (BCM) learning rules: hereafter referred to as the BSTDP rule. In this learning rule, the synaptic weight potentiation is not only driven by the temporal difference between the pre and postsynaptic neuron firing times but also by the postsynaptic neuron activity. We will show in this paper that the BSTDP modulates the height of the plasticity window to establish an input-output mapping (in the learning phase) and also maintains this mapping (via self-repair) if synaptic pathways become dysfunctional. It is the functional dependency of postsynaptic neuron firing activity on the height of the plasticity window that underpins how the proposed SANN self-repairs on the fly. The SANN also uses the coupling between the tripartite synapses and γ-GABAergic (GABA) interneurons. This interaction gives rise to a presynaptic neuron frequency filtering capability which serves to route information, represented as spike trains, to different neurons in subsequent layers of the SANN. The proposed SANN follows a feed-forward architecture with multiple interneuron pathways and astrocytes modulate synaptic activity at the hidden and output neuronal layers. The self-repairing capability will be demonstrated in a robotic obstacle avoidance application and simulation results will show that the SANN can maintain learned manoeuvres at synaptic fault densities of up to 80% regardless of the fault locations.**

***Index Terms*—Spiking neural networks, astrocyte, self-repair, fault tolerance, obstacle avoidance.**

I. Introduction

WHILE state-of-the-art hardware devices and neuromorphic chips [1]–[6] replicate to an extent a brain information processing paradigm, they are not fault-tolerant and can develop faults due to incorrect operations in post-manufacturing [7], wear-out failures [8], or radiation effects [9]. Therefore, fault tolerance is still a key challenge for modern hardware systems. Traditional approaches to address this challenge generally include several stages, e.g. fault detection [7], fault diagnosis [10], and correction/reconfiguration [11], [12]. Additionally, other techniques like redundancy [13], error correction method [14] can also be used to enhance the system fault tolerance. However, most of these approaches are not distributed and require a central control unit which can also be compromised due to faults. It has recently been reported [4], [15], [16] that the coupling of neurons and astrocytes in the brain may provide an elegant solution to this problem. Specifically, a network of excitatory and inhibitory synapses with spiking neurons was employed to develop a self-adaptive strategy for a robotic controller [17]. The authors have proposed a plastic spiking neural network model which was used to develop a fault-resilient robotic controller [18]. The approach of [19] showed that astrocytes have the potential to provide a distributed self-repairing function (e.g. when the spinal cord has injuries).

In this paper, a self-repairing spiking astrocyte neural network (SANN) is proposed where a novel learning rule (BSTDP) combining the spike-timing-dependent plasticity (STDP) and Bienenstock, Cooper, and Munro (BCM) learning rules is used which serves to initiate/suppress the learning process depending on the firing activity of pre and postsynaptic neurons. Specifically, it will be shown that the BSTDP rule is capable of (1): creating an input output mapping during a conventional learning phase and (2): maintaining this mapping in the presence of dysfunctional synaptic connections: this we define as self-repair. The BSTDP rule couples an γ-GABAergic (GABA) interneuron with tripartite synapse [20] which serves to modulate the height of plasticity windows as a function of presynaptic neuron frequency. This capability endows the SANN with a computationally useful frequency filtering capability where spike trains are routed through different synaptic pathways depending on presynaptic frequency. The proposed SANN is applied to a robotic obstacle avoidance task which is a well known benchmark in many robotic laboratories. Results will show, for the first time, that a computational network that captures known interactions between neurons and astrocytes can not only provide a local learning capability, whereby learning commences when either or both pre and postsynaptic neuron become relatively inactive, but also yield a self-repairing capability post learning to maintain learned mappings. Furthermore, results will also desmonstrate that the self-repairing capability of SANN can maintain input-output mappings for a distributed fault density of up to 80%.

This work is part of the EPSRC funded SPANNER project (EP/N007141X/1) (EP/N007050/1).

J. Liu, L. McDaid, J. Harkin, S. Karim are with School of Computing, Engineering and Intelligent Systems, Ulster University, Northern Ireland, United Kingdom, BT48 7JL. (email: j.liu1@ulster.ac.uk, lj.mcdaid@ulster.ac.uk, jg.harkin@ulster.ac.uk, haji_karim-s@ulster.ac.uk)

A. Johnson, A. Millard, J. Hilder, D. Halliday, A. Tyrrell, J. Timmis are with Department of Electronic Engineering, University of York, York, United Kingdom, YO10 5DD. (email: anju.johnson@york.ac.uk, alan.millard@york.ac.uk, james.hilder@york.ac.uk, david.halliday@york.ac.uk, andy.tyrrell@york.ac.uk, jon.timmis@york.ac.uk)

The main contributions of this paper are as follows:

1) A biologically inspired astrocyte-neural network (SANN) and learning rule is proposed. The BSTDP learning rule combines the STDP and BCM learning rules to initiate a conventional learning cycle and maintain learned input-output mappings in the presence of dysfunctional synapses, e.g. failures.
2) The BSTDP rule captures the biological interplay between GABA interneuron, postsynaptic neurons and the plasticity of synapses. This novel interaction gives the SANN the capability to continuously route data, represented in spike train frequencies, to different areas of the SANN and initiate a repair process in the presence of faults.
3) The fault tolerance of the proposed SANN architecture is evaluated through simulations using a robotic application. Results demonstrate the resilience of the SANN-based robotic controller in an obstacle avoidance application under various fault densities.

The rest of paper is organized as follows. Section II provides the background and motivation. Section III presents SANN models, the BSTDP learning rule and network structure. Section IV provides simulation results that demonstrate the performance of the SANN-based robotic controller under various fault densities and conditions. Section V concludes and gives insight into the potential directions for the future work.

II. Background and Motivation

Astrocytes in the central nervous systems can encapsulate about ten thousand synapses and multiple neurons (e.g. $\sim$6 in the cortex) [21]. These cells interact with synapses and neurons to modulate synaptic activity [22], namely the tripartite synapse [23]. It has been shown that at the tripartite synapse, the astrocyte cells perform a distributed and fine-grained repair [15], see Fig. 1, whereby when synapses are damaged, the Probability of neurotransmitter Release (PR) at synapses drops which leads to fall off in the activity at postsynaptic neurons. However, it is now commonly known that a negative feedback signal, often referred to as the retrograde messengers (endocannabinoids) pathway, exists where the messengers are synthesised by active postsynaptic neurons. This retrograde messenger forms an indirect signalling pathway which increases the PRs of the all functional synapses associated with postsynaptic neurons enabling the recovery of the postsynaptic firing rate [15]. We define this process as the self-repair and the indirect retrograde messenger is the key catalyst.

This self-repairing mechanism has been implemented in an electronic hardware system [4] and unlike existing fault tolerance techniques (e.g. triple modular redundancy and error correction technique) the self-repairing astrocyte-neural network has shown promise as an effective adaptive computational paradigm as it is not dependant on a central controller. Furthermore, it has been demonstrated that this self-repairing approach can maintain the system functionality for both localised and distributed faults (up to 40% fault densities), and performance degrades by only 20% if the network is seriously damaged by a fault density of 80% [4]. This hardware architecture was optimized for the low area overhead [24] and achieved less hardware resource utilization than the original work of [4], therefore provides an efficient design solution for large scale networks. A small SANN has been applied to a mobile robotic car application [25] with a fixed input spike train. However, the work in this paper goes much further and proposes a SANN for a more complex robotic task in that the SANN takes on the role of a controller where input-output mappings are initially learned, allowing the robot to navigate around a series of obstacles. Furthermore, the SANN controller maintains the obstacle avoidance capability when faults occur. To the best of the authors' knowledge, this is the first time that a network combining astrocytes with neurons has been shown to implement a learning and fault-tolerant capability which can be harnessed in a challenging application.

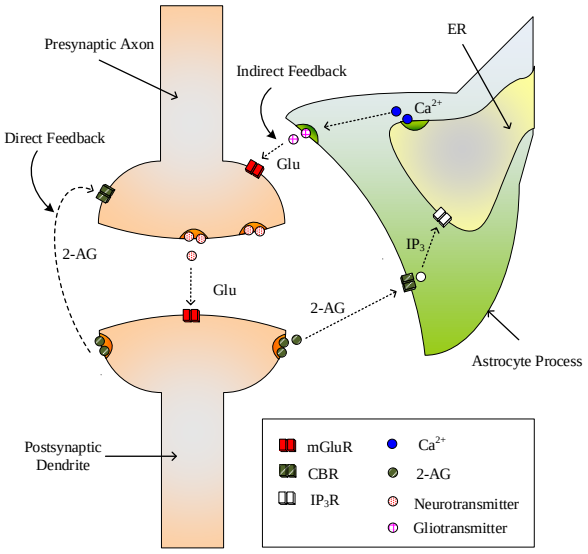

Fig. 1. A tripartite synapse where the direct feedback is from the postsynaptic dendrite, and the indirect feedback is from the astrocyte cell [15].

III. Self-repairing Astrocyte Neural Network Model

In this section, the SANN architecture is presented together with the BSTDP learning rule and neuron/synaptic models. Specifically, we will start with communication between excitatory neurons, GABA neurons and astrocytes at tripartite synapses. From this we will distil out biological realistic models that capture the essence on the biological interplay between these cells while at the same time minimising the computational overhead.

A. Activity-dependent Mechanism in the Tripartite Synapses

Recent research shows that the GABA interneuron participates in the activities of neurons and synapses [26] where for low presynaptic frequencies the GABA interneuron has an inhibitory affect on the presynaptic neuron. The signalling pathways between the GABA interneuron and tripartite synapse are shown in Fig. 2. The conventional tripartite synapse has three

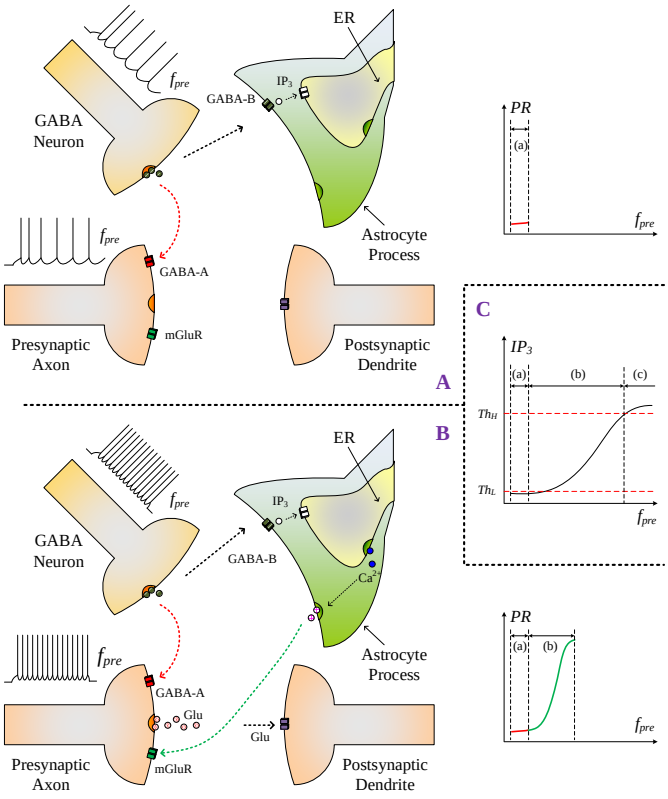

Fig. 2. Signalling interactions between a tripartite synapse and a GABA interneuron. (A). A low f_{pre}. (B). A high f_{pre}. (C). IP_3 versus f_{pre}.

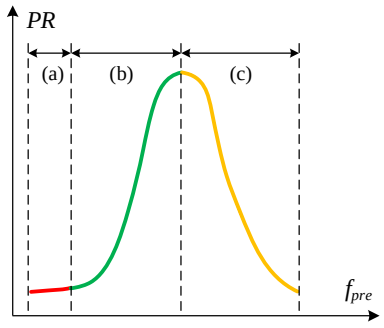

Fig. 3. Spike frequency f_{pre} vs synaptic PR for a tripartite synapse and GABA interneuron. In the stage (a), the low f_{pre} is insufficient to cause the release of Ca^{2+} in the astrocyte, and no gliotransmitter is released. Thus the PR is low due to the inhibitory effect from the GABA interneuron. For the stage (b), as the f_{pre} is high, the IP_3 is sufficient (reaching the the low threshold Th_L) to trigger the release of Ca^{2+}. The gliotransmitter is released which overcomes the inhibitory effect of the GABA, thus the PR is increasing. In the stage (c), the f_{pre} is too high and causes the IP_3 reaching the upper threshold Th_H. It stops the release of Ca^{2+} and no gliotransmitter binds to the mGluR at the presynaptic terminal, which causes the inhibitory effect of GABA to be dominant again and the PR decreases.

terminals shown by Fig. 1, which are the presynaptic axon, the postsynaptic dendrite and the astrocyte cell. However, the GABA interneuron introduces an additional terminal and we now consider this. When a spike train of frequency (f_{pre}) arrives at the presynaptic axon, the neurotransmitter (in this case glutamate) is released from cleft. It binds to the receptors at the postsynaptic dendrite, which depolarizes the postsynaptic neuron. The spikes presenting at the presynaptic axon also arrive at the GABA interneuron [26] causing GABA to be released which subsequently binds to GABA-B receptors at the astrocyte cell. This triggers the release of inositol 1, 4, 5-trisphosphate (IP_3). For a low f_{pre} shown in Fig. 2A, the amount of released IP_3 is insufficient to cause the release of calcium Ca^{2+} from the Endoplasmic Reticulum (ER) due to degradation of the IP_3. Thus no Ca^{2+}-induced glutamate is released from the astrocyte. However, GABA also binds to the GABA-A receptors at the presynaptic terminal which has an inhibitory effect causing a low PR at the tripartite synapse, as shown in Fig.2A (red line): PR remains low for low f_{pre}. As f_{pre} is increased, as shown in Fig. 2B, more GABA binds to the GABA-B receptors and at some "trigger" frequency a sufficient amount of IP_3 is released to overcome IP_3 degradation and a low IP_3 threshold Th_L is reached, causing Ca^{2+} released from the ER and a subsequent Ca^{2+} transient. The release of Ca^{2+} results in Ca^{2+}-induced glutamate release which subsequently binds to group I metabotropic Glutamate Receptors (mGluR) at the presynaptic terminal. It overcomes the inhibitory effect of GABA-A leading to an increase in PR of the presynaptic terminal, see Fig. 2B (green line). If f_{pre} continues to increase, the IP_3 within the astrocyte also increases and eventually reaches the upper threshold Th_H, as shown in Fig. 2C, and the oscillatory Ca^{2+} transient ceases. In this case glutamate is no longer released causing the inhibitory effect of GABA-A to be dominant again and the PR decreases at presynaptic terminal, see Fig. 3 (yellow line). Therefore, the interactions between the inhibitory GABA interneuron and the astrocyte can give rise to a frequency selective PR behaviour at tripartite synapses. This behaviour points towards a "band-pass" filtering characteristic for presynaptic spike trains where the passband will be closely related to cellular morphology, receptor distribution and many other aspects. Therefore, we assume that, as morphology and receptor density differs across synaptic sites, there will be a spread in the centre frequency of bandpass filters across the SANN, which will give rise to an advantageous SANN signal routing capability (This is discussed later in the paper). Effectively what is being filtered is the release of glutamate where with PR approaching unity, almost every spike arriving at a presynaptic terminal will cause the release of glutamate. Consequently, with the rapid arrival of glutamate in the cleft a strong STDP based learning phase occurs. However, as PR drops then fewer spikes release glutamate and the plasticity of synapses falls. Therefore, we propose that PR is effectively a local switch which can turn on/off learning at synaptic sites by modulating the height of the plasticity window: as $PR \rightarrow 1$ the plasticity window fully opens and with $PR \rightarrow 0$ the window closes. Section III-D of this paper proposes that activity at postsynaptic neurons also controls the plasticity of synapses.

To avoid the computational complexity discussed in Fig. 2, the interactions between GABA and the tripartite synapse can be approximated by a Gaussian function, which is shown by Fig. 3. It can be seen that the synaptic PR is a function of f_{pre}, where the three stages of (a)-(c) correspond to the descriptions outlined in Fig. 2.

The Gaussian function in Fig. 3 is described by

$$PR = e^{-\frac{(f_{pre} - f_s)^2}{2\sigma^2}}, \quad (1)$$

where f_s is the sensitive (centre) frequency of the presynaptic terminal, σ is the width of Gaussian passband: both of these parameters are set by encoding scheme.

B. Neuron Model

Previous research have proposed several spiking neuron models, such as Hodgkin-Huxley model [27] and FitzHugh-Nagumo model [28], [29]. However, these models are computing-intensive as they used complex mathematics to describe the biological behaviours of the neuron [30]. Thus simplified models, including the Izhikevich [31] and Leaky Integrate-and-Fire (LIF) models [32], were proposed and are now widely used in many approaches [33]–[35]. In this paper, the simplified neuron model of LIF [32] is used, which is given by

$$\tau_m \frac{dv}{dt} = -v(t) + R_m \sum_{i=1}^{n} I_{syn}^i(t), \quad (2)$$

where v is the membrane potential of the neuron, I_{syn}^i is the injected current from i^{th} synapse and the total number of synapse is n. The parameter descriptions of τ_m, R_m and v_{th} and their values in this work can be found in Table I. The neuron goes to the refractory period when $v > v_{th}$ and the refractory period is $\sim$2 ms in this approach.

C. Synapse Model

In this work, a probabilistic-based model is used for the synapses, which is based on the synaptic neurotransmitter releasing mechanism similar to the approaches of [15], [36]. In this model when a pre-synaptic spike presents at the synapse, a random number generator generates a value $rand$ (between 0 and 1) which is used to compare with PR of the synapse. If $rand \leq PR$, the synaptic current is generated, which is described by

$$I_{syn}^i(t) = \begin{cases} r_I * w_{syn}^i(t)/n, & rand \leq PR \\ 0, & rand > PR \end{cases} \quad (3)$$

where $rand$ is the generated random number, r_I is the current production rate, w_{syn}^i is the weight of the i^{th} synapse associated with neuron. All the parameters for the neuron and synapse models can be found in Table I.

TABLE I
NEURON, SYNAPSE MODEL PARAMETERS

Parameters	Parameter description	Value
τ_m	Neuron membrane time constant	240 ms
R_m	Neuron membrane resistance	1.2 GΩ
v_{th}	Firing threshold value	9 mv
r_I	Synaptic current production rate	8

D. BSTDP Learning Rule

In this paper, a new learning algorithm with the capability of not only mapping new input data patterns to a desired output pattern, but also sensing when synaptic pathway(s) becomes dysfunctional and initiating re-learning or repair, was developed. If synaptic connections become broken or damaged, the corresponding currents injected into the neuron diminishes, which will reduce or even cause the firing activity of the postsynaptic neuron to cease. The BSTDP continually monitors the activity of postsynaptic neurons and when the level of activity of these neurons drops below a predetermined threshold a feedback signal initiates a localised learning phase. As learning process progresses, the activity of postsynaptic neuron increases which strengthens this indirect retrograde signalling pathway resulting in an increase in the astrocytic IP_3. With sufficiently high postsynaptic activity astrocytic IP_3 concentration will cross the upper IP_3 threshold and the Ca^{2+} transient ceases. Thereafter, no glutamate is released and PR falls off to a low background level resulting is shut down of learning: the plasticity window in (5) has collapsed. Hence as astrocytic IP_3 can be elevated from either direct signals by GABA interneurons or the indirect retrograde pathway originating from the postsynaptic neuron then both the pre and postsynaptic activity modulate the plasticity at synaptic sites. Consequently even if the frequency of the presynaptic neuron f_{pre} is fixed and falls within the bandpass range, as outlined in Fig.2, the plasticity window will only open if the postsynaptic neuron activity is below a predefined maximum. Effectively the height of PR in Fig.2 is modulated by the postsynaptic neuron frequency and this leads the authors to propose that the link between postsynaptic neuron activity, PR and synaptic plasticity may explain the biophysical processes underpinning the BCM learning function. Furthermore, there is strong experimental evidence for this feedback pathway where it has been shown [15], [26] that the retrograde messenger (endocannabinoids), which are synthesised in active postsynaptic neurons, act as an indirect signalling messenger, via astrocytes and the IP_3 pathway, that modulates PR, and hence plasticity, at local and distal synapses.

However, due to the computational overhead that would be incurred in modelling this feedback pathway and also its causal effect is adequately captured in the BCM function, we adopt the BCM model to map postsynaptic neuron activity directly to the plasticity of synapses. Hence, we now formulate a model for the BSTDP rule that merges conventional STDP learning with the proposed indirect pathway (BCM). The BSTDP rule updates the synaptic weights according to the timing difference between the pre and postsynaptic spikes, and is described by

$$\delta w(\Delta t) = \begin{cases} A_0 exp(\frac{\Delta t}{\tau_+}), & \Delta t \leq 0 \\ -A_0 exp(\frac{\Delta t}{\tau_-}), & \Delta t > 0 \end{cases} \quad (4)$$

where $\delta w(\Delta t)$ is used to update the synaptic weight, Δt is the time difference between presynaptic and postsynaptic spikes, A_0 is the plasticity window height, τ_+, τ_- control the width of the plasticity window, and they are $40ms$ in this approach.

Since the indirect feedback pathway appears to underpin the BCM rule we can use the established BCM function to model the relationship between postsynaptic activity and plasticity at synapses, as follows. The height of the plasticity window A_0 is modulated by a BCM type behaviour using the actual and target postsynaptic firing rates according to

$$A_0 = \frac{A}{1 + e^{a(f - f_o)}} - A_-, \tag{5}$$

where A is the maximum plasticity window height, A_- is the maximum plasticity window height for depression, f and f_o are the actual firing rate (i.e. a running average over forty seconds) and target firing rate of the postsynaptic neuron, respectively. The parameter a controls the plasticity window opening and closing rates and was set to 0.2 in this work. All the parameters for the BSTDP learning rule can be found in Table II.

When $f \gg f_o$, then $A_0 \approx A_-$, which leads to long-term depression (LTD) and for $f \ll f_o$, $A_0 \approx A - A_-$, which gives rise to long-term potentiation (LTP). It is clear that if the postsynaptic neuron is in the early learning phase or the firing rate drops off due to the faulty synaptic connections, then the plasticity window height A_0 is positive (the learning window is open). This initiates a learning phase where the synaptic weights of the remaining non-dysfunctional synapses potentiate, eventually stabilising when the neural firing rate f approaches f_o. Thus when faults occur and f diminishes, this process will recover the postsynaptic neuronal firing rate to the pre-fault level. This is the self-repairing process which will be shown in the next section to maintain the functionality of the network when the synapses are damaged or broken. The results under various faulty conditions will also be provided to demonstrate this capability.

E. Self-repairing SANN architecture

The proposed SANN follows the architecture of feed forward neural networks. Fig. 4(a) is an example of the SANN architecture which includes an input, a hidden, and an output layers. Note that we have now modelled the interaction between the GABA neuron and the tripartite synapse as a Gaussian function: hereafter referred to as "Gaussian" synapses. The SANN uses multiple pathway connections, between neurons in different layers, with different delays for each pre and post neuron pairing, as shown by Fig. 4(b). Multiple pathways with delays are required to facilitate spatial data for the formation of a postsynaptic potential. Note that Fig. 4(a) is an example with only one hidden layer, but the SANN could also include multiple hidden layers.

In the proposed SANN information is passed from layer to layer in a forward direction where the input sensor data is encoded into spike trains (see later). Neurons in the middle and output layers have an associated Gaussian passband, implemented using (1) and (5), and therefore each neuron exhibits a unique "receptive field". For example, consider the case for the SANN in Fig. 4(a) where there are n unique input patterns. Each pattern is assigned to a single neuron in the hidden layer and therefore this layer will contain n neurons where each of these neurons has a receptive field associated with one of the n input patterns. This association is achieved using the centre frequency $f = f_s$ of the Gaussian function whereby a different f_s value is used for each Gaussian synapse and this spread in f_s will be sensitive to a unique input pattern: because of this spread in f_s each of hidden layer neurons will be associated with one only possible input pattern. Hence in Fig. 4(a) the three input spike patterns can be accommodated with a corresponding mapping to the output layer neurons.

In real networks many processing neurons exist where groups of these neurons will be sensitive to different input patterns. Therefore, in these networks there is likely to exist neuron grouping that is receptive to a particular pattern where some will fire maximally to the pattern while others less so. It may even be possible to tune a neuron receptive fields as the shape of a receptive field is defined by the synaptic inputs to that neuron. These local or lateral connections are often inhibitory and by adjusting the associated weights it is conceivable that part of the transmitted information could be removed. However, this is beyond the scope of this paper and because of the computational overhead we restricted the number of hidden layer neurons by setting their receptive fields to match known input patterns.

TABLE II
BCM-STDP LEARNING RULE PARAMETERS

Parameters	Parameter description	Value
A	Window height of LTP+LTD	1
A_-	Window height of LTD	0.5
a	Constant	0.2
τ_+	LTP plasticity window	40 ms
τ_-	LTD plasticity window	40 ms

IV. SIMULATION RESULTS

The test bench setup is discussed followed by simulation results which show the performance of the SANN in an obstacle avoidance task. This task is employed as an example to demonstrate how the SANN can self-adapt to different fault conditions. The simulation results are provided from software simulations of the biological SANNs. Then the hardware acceleration is discussed in the final subsection which demonstrates the possibility of deploying the SANN to real-world robotic hardware platforms.

A. Example Application Setup

The obstacle avoidance data was collected using the Psi swarm robot shown in Fig. 5 which was developed by the York Robotics Laboratory, University of York, UK [37]. In this task, four infrared sensors were used with one at the front, one at each side (right and left) and one at the back where each sensor provided the sensory input data for the SANN controller, and the SANN output neurons gave the commands to drive the motors. The Psi swarm robot was deployed and the sensory data and corresponding controller decisions were recorded to local memory on the robot, and then downloaded

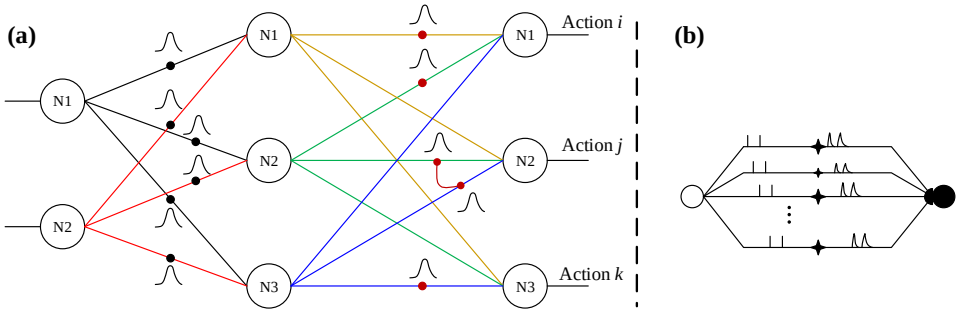

Fig. 4. An SANN example is shown by (a) where a pair of neurons is connected by "Gaussian" synapses, and (b) shows the multiple pathways of the synaptic connections between the pre and postsynaptic neurons.

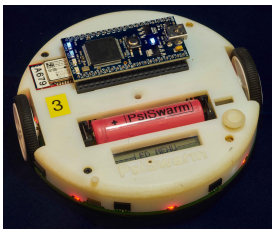

Fig. 5. The Psi swarm robot developed by York Robotics Laboratory, University of York.

after the experiments. Moving forward is the default action for the robot and it has the highest priority whereas moving backward has the lowest priority. Thus the action priorities are $F > R > L > B$, where F/R/L/B represent moving forward, turning right, left and moving backward, respectively.

In this work sensors have a threshold level at which an object is detected and for sensory levels above this threshold the sensor value is mapped to a linear spike train frequency of 35 Hz, otherwise the mapping is to a frequency of 25 Hz. The output layer has four neurons corresponding to the four possible actions that can be taken by the Psi swarm robot to avoid obstacles. The target firing rates for the neurons in the hidden and output layers were arbitrarily set to 25 Hz and 10 Hz, respectively. Each synaptic connection has multiple pathways which are 8 and 16 for the connections in the hidden and output layers, respectively. Each synaptic pathway is delayed by 1 ms from the neighbouring pathway. Thus the minimum delay of a pathway is zero and the maximum is 7 ms and 15 ms for hidden and output layers, respectively: these delay times were arbitrarily chosen. The SANN architecture is given by Fig. 6 and each sensory neuron in the hidden layer generates an input spike train and in this simulation, the maximum number of possible input spike train in a pattern is 15: no action is needed when all sensors are activated as the Psi swarm robot is trapped.

B. No Fault Condition

Consider the scenario where there is an obstacle directly in the front of the robot (denoted by pattern A in Fig. 6) which would give rise to an input spike train of 35, 25, 25, and 25 Hz across all four sensory neurons. As this pattern matches the spread in f_s across synapses associated with neuron #9 in the hidden layer then the plasticity window for these synapses will open and learning will be initiated and continue until neuron #9 reached a predefined firing frequency of 25 Hz. Fig. 7(a) shows that this is indeed the case where its firing rate increases gradually during the learning phase and eventually at around 170 s the firing rate of neuron #9 reaches 25 Hz and thereafter stabilises. The corresponding weights associated with neuron #9 potentiated during this learning phase, as shown in Fig. 7(b), and also stabilise at $\sim$170 s because at 25 Hz the plasticity window closes and learning ceases. Activity at neuron #9 must be mapped to an action where the next highest priority is turning right, and we associated this action with neuron #2 in the output layer. Fig. 7(c) shows that the neuron #2 begins firing at $\sim$150 s and this is because a period of learning is required before the weights associated with neuron #2 are potentiated to a level whereby the postsynaptic potential is sufficient to cause firing of neuron #2: note that STDP learning takes place for all synapses associated with neuron #2 even for subthreshold postsynaptic potentials due to Slow Inward Currents (SICs) as a result of Ca^{2+} activity in the nearby astrocyte. The synaptic weights associated with neuron #2 are shown in Fig. 7(d) and again it can be seen that these weights are potentiated and stabilise after a period of learning: as neuron #2 firing rate approaches the target frequency of 10 Hz (Fig. 7(c)) the learning window closes and finally the associated synaptic weights stabilize. Additional results (not provided due to space) demonstrated that none of the remaining output neurons were active for this input firing pattern.

Fig. 7 shows the SANN learning process under the input pattern A, i.e. an obstacle is directly in front of the robot. When the input pattern changes to pattern B, obstacles are placed at both the front and right side of the robot. This pattern is uniquely associated, through the spread in the centre frequencies of the Gaussian synapses, with neuron #13 in the hidden layer and neuron #3 in the output layer. In the same way as for pattern A, synapses associated with both these neurons begin to potentiate until both neurons reach their target frequency and a similar learning process takes place for all other patterns. Therefore, after a period of training across all possible input patterns, the SANN will have implemented a mapping between input patterns generated by the sensory neurons and the output neurons. For the purposes of demonstrating the SANN under fault conditions we now

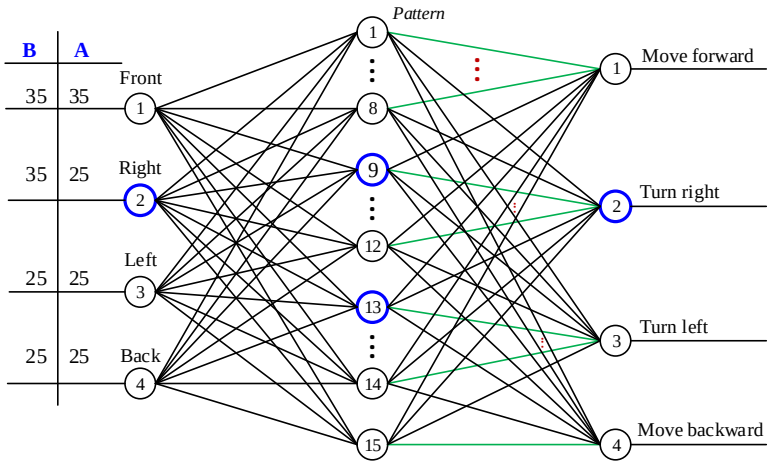

Fig. 6. SANN architecture for the obstacle avoidance task. A and B are possible encoding schemes for two input patterns.

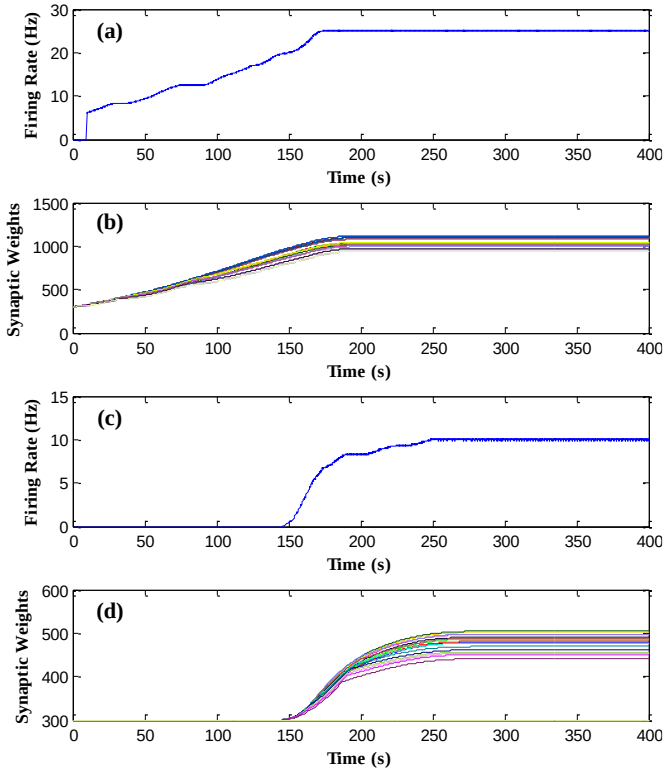

Fig. 7. Firing rates and synaptic weights of the SANN. (a, b) are the firing rate and synaptic weights of neuron #9 of the hidden layer while (c, d) are the firing rate and synaptic weights of neuron #2 of the output layer.

fix all the weights across the SANN at their post trained values and in the next section we present simulation results that demonstrate how the SANN maintains this mapping under fault conditions.

C. Fault Condition

Consider the case where pattern A is presented to the SANN, and at $t = 600$ seconds, seven of the eight pathways linking neuron #2 in the input layer with neuron #9 in the hidden layer developed faults: in this work we implement a fault on a pathway by permanently setting PR to zero. At the same time eight of the sixteen pathways linking neuron #9 in the hidden layer with neuron #2 in the output layer also developed faults. This reduces the activity at both neuron #9 in the hidden layer and neuron #2 in the output layer. Fig. 8(a) shows the firing rate of the neuron #9 of hidden layer and it can be seen that this rate drops off to ∼20 Hz from its target frequency of 25 Hz due to the introduction of the above faults. This frequency difference causes the plasticity window to reopen (modelled by (5)) and re-learning or repair commences (modelled by (4)). Fig. 8(b) shows that during this repair process the synaptic weights associated with neuron #9 potentiate over a "repair" period of 600 to ∼700 seconds and thereafter remain stable as the firing rate of this neuron reaches its target value of 25 Hz. The drop in the firing rate of neuron #2 in the output layer (see Fig. 8(c)) is much more significant as half of the associated synaptic pathways are broken and, in addition, the output spike frequency of neuron #9 in the hidden layer has reduced due to damage in the hidden layer. Fig. 8(c) shows the recovery in the activity of neuron #2 to its pre-fault level (10 Hz) and again this occurs due to re-training which causes the remaining healthy (undamaged) synaptic pathways to potentiate, as shown by Fig. 8(d).

Now consider the case where faults are scattered randomly across the SANN with a fault density of 40%. The aim of this simulation is to evaluate how well the SANN maintains input-output mappings with a network-wide distribution of faults. Four different input patterns were presented to the SANN where each pattern activates a different output neuron. Fig. 9 shows the firing rates of all four output neurons where it can be seen that after faults occur, the firing rate of all four neurons drop significantly, but after a period of re-learning or repair these neurons become active again and eventually reach their target firing rate. Note that the recovery time of each output neuron is different and this correlates with the fault distribution: the causal effect of the drop in activity of a hidden layer neuron will be different across all fours output neurons. This results clearly demonstrate the ability of the

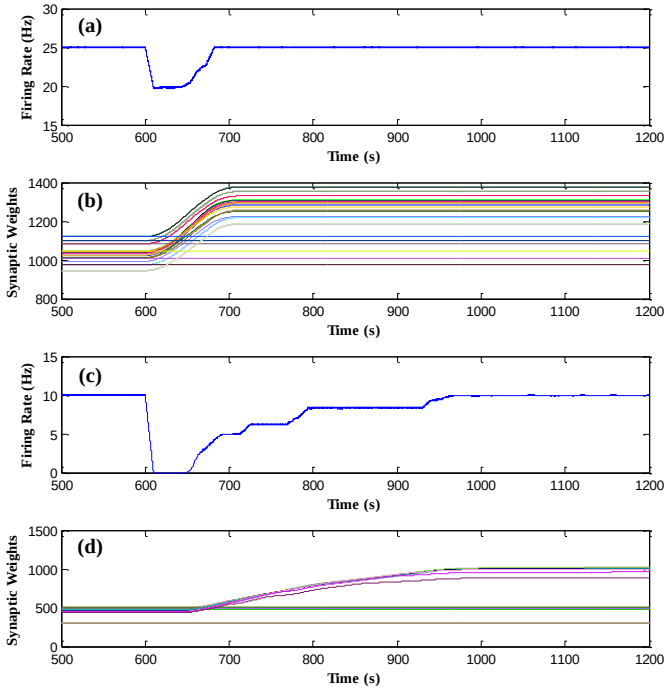

Fig. 8. Simulation results when faults occur. (a, b) are the firing rate and synaptic weights of neuron #9 in the hidden layer while (c, d) are the firing rate and synaptic weights of neuron #2 in the output layer.

SANN to recover from a scattering of faults.

D. Fault densities variations

The fault tolerance capability of the SANN was also evaluated for different fault densities. The fault density is defined as the percentage of the dysfunctional (faulty) synapses against the total number of synapses. In this simulation, only pattern A is used as the input and faults were localised to pathways between the input sensory neuron #2 and neuron #9 in the hidden layer. Faults were set to occur at 300 seconds and two metrics were used to evaluate the self-repairing performance of the SANN: the lowest firing rate (f_L) of a neuron after a fault occurs, which reflect the severity of the faults on neuronal activity, and the fault recovery period (T_R) which reflects the recovery period or speed of recovery. The SANN was evaluated under fault densities of 20%, 40% and 80%. Fig. 10 shows the fault recover characteristics for neuron #9 in the hidden layer. It can be seen clearly from this plot both the neuronal activity and the repair duration correlate with the fault density.

Table III gives the f_L and T_R for neuron #9. As more synaptic connections become dysfunctional the longer the recovery time, as expected. However, despite the correlation between recovery time and faults density, the SANN does recover its functionality even under a high-density fault condition.

E. Hardware acceleration of the SANN

Note that the recovery time of 20-65 seconds in Section IV-D is in terms of biological time but it can be accelerated

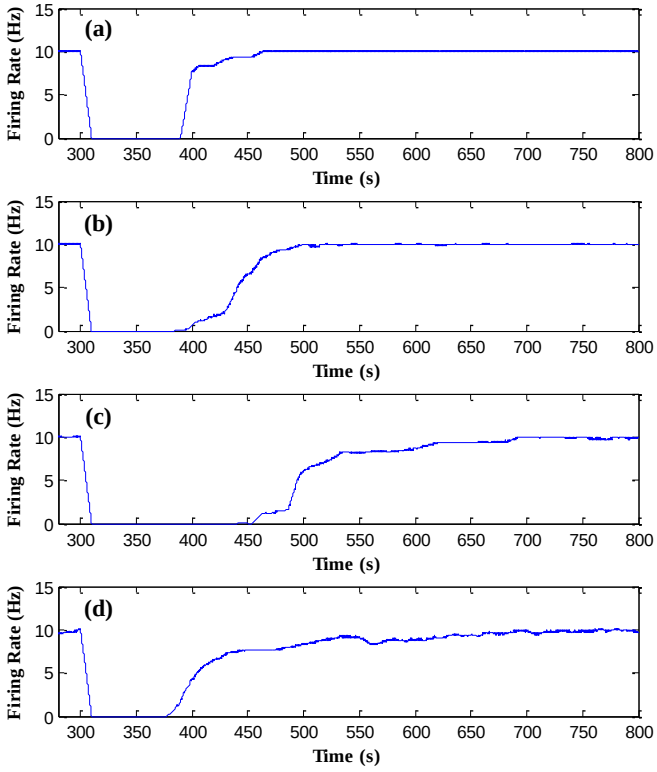

Fig. 9. Simulation results under 40% fault density across the network. (a)-(d) show the firing rates of neuron #1-#4 of the output layer, respectively.

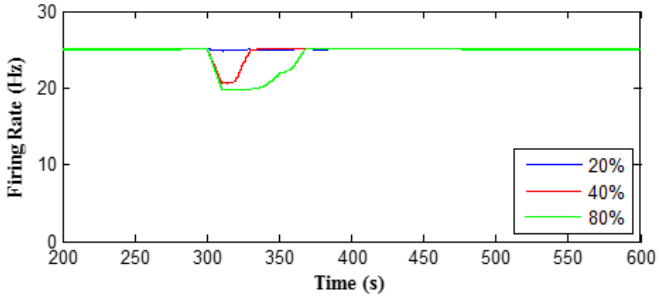

Fig. 10. Firing rate of the neuron #9 of hidden layer under various fault densities.

with hardware implementations. Based on the authors' previous works of [4], [24], the FPGA implementation of an SANN can execute at clock speeds of 10-50 MHz, where one clock period is matched to one millisecond of the biological time step. Therefore, the recovery time of 65 seconds in biology would only require 6.5 ms when implemented on FPGA hardware, so this is within real-time constraints for many visual processing applications. This achieves an acceleration rate of 10^4 thus making this approach viable for real-time implementations of fault tolerance hardware. This is one direction of future work currently under investigation.

In summary, compared to conventional fault tolerance approaches, the proposed method has several advantages including: a). A distributed fault-resilient mechanism. The proposed SANN is a distributed neural network which does not require a

TABLE III
THE f_L AND T_R OF THE NEURON #9 OF HIDDEN LAYER UNDER VARIOUS FAULT DENSITIES

Fault density	f_L (unit: Hz)	T_R (unit: s)
20%	24.6	20
40%	20.5	35
80%	19.8	65

centre controlling unit and therefore the SANN demonstrates a higher degree of fault tolerance; b). Fine-grained fault-tolerant mechanism. The SANN supports repair at the level of synapses which, when compared to other more conventional approaches, is at a basic component or multi-transistor (logic gate) level. We view this as fine grained when compared to, for example, the approach in [38], where the entire column inside the FPGA device is reconfigured during partial reconfiguration (i.e. this is very much coarse-grain repair); and finally c). Low cost/overhead where unlike the redundancy [13] (e.g. triple modular redundancy), error detection/correction [7], [11] methods etc., the SANN does not require additional components to detect and repair faults. Therefore, the proposed SANN architecture can provide a low cost, distributed, fine-grained fault-tolerant route to autonomous hardware.

V. CONCLUSION

A distributed self-repairing spiking astrocyte neural network with an information routing capability, underpinned by known interaction between an inhibitory GABA interneuron coupled with a tripartite synapse, has been presented in this paper. To minimise the computational overhead this interaction was realised in a Gaussian synaptic function which serves to route spike trains of different frequencies to different parts of the network. Furthermore, a biologically plausible link between postsynaptic neuron frequency and the probability of neurotransmitter release at synaptic sites was proposed and captured in the BSTDP learning rule, which combines the conventional STDP with the BCM rule. The paper has demonstrated that the rule provides a novel self-repairing capability which can not only establish an initial mapping between input data patterns and desired output response but also maintains this mapping in the presence of both localised or globally distributed faults. The fault-tolerant capability of the SANN was demonstrated in an obstacle avoidance task with results demonstrating that pre-learned input/output mappings can be maintained for fault densities up to 80% regardless of whether the faults are localised or globally distributed. Future work will apply the SANN to the domain of robotics for mission critical tasks and swarm applications. In these applications the robots' functions can be compromised due to faults (such as caused by radiations, component ageing etc.), therefore fault tolerance is an extremely important capability in maintaining the key functionality of robotic and other hardware systems.

REFERENCES

[1] R. F. Service, "The brain chip," *Science*, vol. 345, no. 6197, pp. 614–616, 2014.

[2] B. V. Benjamin, P. Gao, E. McQuinn, S. Choudhary, A. R. Chandrasekaran, J. M. Bussat, R. Alvarez-Icaza, J. V. Arthur, P. a. Merolla, and K. Boahen, "Neurogrid: A mixed-analog-digital multichip system for large-scale neural simulations," *Proceedings of the IEEE*, vol. 102, no. 5, pp. 699–716, 2014.

[3] S. B. Furber, D. R. Lester, L. A. Plana, J. D. Garside, E. Painkras, S. Temple, and A. D. Brown, "Overview of the SpiNNaker system architecture," *IEEE Transactions on Computers*, vol. 62, no. 12, pp. 2454–2467, 2013.

[4] J. Liu, J. Harkin, L. P. Maguire, L. J. Mcdaid, and J. J. Wade, "SPANNER: A self-repairing spiking neural network hardware architecture," *IEEE Transactions on Neural Networks and Learning Systems*, vol. 29, no. 4, pp. 1287–1300, 2018.

[5] T. Chen, Z. Du, N. Sun, J. Wang, C. Wu, Y. Chen, and O. Temam, "DianNao: A small-footprint high-throughput accelerator for ubiquitous machine-learning," in *19th International Conference on Architectural Support for Programming Languages and Operating Systems*, 2014, pp. 269–284.

[6] Y. Chen, T. Luo, S. Liu, S. Zhang, L. He, J. Wang, L. Li, T. Chen, Z. Xu, N. Sun, and O. Temam, "DaDianNao: A machine-learning supercomputer," in *Annual International Symposium on Microarchitecture (MICRO)*, 2015, pp. 609–622.

[7] J. Liu, J. Harkin, Y. Li, and L. Maguire, "Online traffic-aware fault detection for Networks-on-Chip," *Journal of Parallel and Distributed Computing*, vol. 74, no. 1, pp. 1984–1993, 2014.

[8] M. Radetzki, C. Feng, X. Zhao, and A. Jantsch, "Methods for fault tolerance in Networks-on-Chip," *ACM Computing Surveys*, vol. 46, no. 1, pp. 1–38, 2013.

[9] F. Siegle, T. Vladimirova, J. Ilstad, and O. Emam, "Mitigation of radiation effects in SRAM-based FPGAs," *ACM Computing Surveys*, vol. 47, no. 2, pp. 1–34, 2015.

[10] A. Ghofrani, R. Parikh, S. Shamshiri, A. DeOrio, C. Kwang-Ting, and V. Bertacco, "Comprehensive online defect diagnosis in on-chip networks," in *IEEE 30th VLSI Test Symposium (VTS)*, 2012, pp. 44–49.

[11] J. Liu, J. Harkin, Y. Li, and L. P. Maguire, "Fault tolerant Networks-on-Chip routing with coarse and fine-grained look-ahead," *IEEE Transactions on Computer-Aided Design of Integrated Circuits and Systems*, vol. 35, no. 2, pp. 260–273, 2016.

[12] W. Barker, D. M. Halliday, Y. Thoma, E. Sanchez, G. Tempesti, and A. M. Tyrrell, "Fault tolerance using dynamic reconfiguration on the POEtic tissue," *IEEE Transactions on Evolutionary Computation*, vol. 11, no. 5, pp. 666–684, 2007.

[13] I. Pomeranz and S. M. Reddy, "Robust fault models where undetectable faults imply logic redundancy," *IEEE Transactions on Very Large Scale Integration (VLSI) Systems*, vol. 18, no. 8, pp. 1230–1234, 2010.

[14] K. S. Morgan, D. L. McMurtrey, B. H. Pratt, and M. J. Wirthlin, "A comparison of TMR with alternative fault-tolerant design techniques for FPGAs," *IEEE Transactions on Nuclear Science*, vol. 54, no. 6, pp. 2065–2072, 2007.

[15] J. Wade, L. McDaid, J. Harkin, V. Crunelli, and S. Kelso, "Self-repair in a bidirectionally coupled astrocyte-neuron (AN) system based on retrograde signaling," *Frontiers in Computational Neuroscience*, vol. 6, no. 76, pp. 1–12, 2012.

[16] M. Naeem, L. J. McDaid, J. Harkin, J. J. Wade, and J. Marsland, "On the role of astroglial syncytia in self-repairing spiking neural networks," *IEEE Transactions on Neural Networks and Learning Systems*, vol. 26, no. 10, pp. 2370–2380, 2015.

[17] J. Liu, J. Harkin, M. McElholm, L. McDaid, A. Jimenez-Fernandez, and A. Linares-Barranco, "Case study: Bio-inspired self-adaptive strategy for spike-based PID controller," in *IEEE International Symposium on Circuits and Systems (ISCAS)*, 2015, pp. 2700–2703.

[18] A. P. Johnson, J. Liu, A. G. Millard, S. Karim, A. M. Tyrrell, J. Harkin, J. Timmis, L. J. McDaid, and D. M. Halliday, "Homeostatic fault tolerance in spiking neural networks A dynamic hardware perspective," *IEEE Transactions on Circuits and Systems*, vol. 65, no. 2, pp. 687–699, 2018.

[19] T. A. Fiacco, C. Agulhon, and K. D. McCarthy, "Sorting out astrocyte physiology from pharmacology," *Annual Review of Pharmacology and Toxicology*, vol. 49, no. 1, pp. 151–174, 2009.

[20] A. Araque, G. Carmignoto, P. G. Haydon, S. H. R. Oliet, R. Robitaille, and A. Volterra, "Gliotransmitters Travel in Time and Space," *Neuron*, vol. 81, no. 4, pp. 728–739, 2014.

[21] M. M. Halassa, T. Fellin, H. Takano, J.-H. Dong, and P. G. Haydon, "Synaptic islands defined by the territory of a single astrocyte," *The Journal of Neuroscience*, vol. 27, no. 24, pp. 6473–6477, 2007.

[22] B. Stevens, "Neuron-astrocyte signaling in the development and plasticity of neural circuits," *Neurosignals*, vol. 16, no. 4, pp. 278–288, 2008.

[23] A. Araque, V. Parpura, R. P. Sanzgiri, and P. G. Haydon, "Tripartite synapses: Glia, the unacknowledged partner," *Trends in Neurosciences*, vol. 22, no. 5, pp. 208–215, 1999.
[24] A. P. Johnson, D. M. Halliday, A. G. Millard, A. M. Tyrrell, J. Timmis, J. Liu, J. Harkin, L. Mcdaid, and S. Karim, "An FPGA-based hardware-efficient fault-tolerant astrocyte-neuron network," in *IEEE Symposium Series on Computational Intelligence*, 2016, pp. 1–8.
[25] J. Liu, J. Harkin, L. Mcdaid, D. M. Halliday, A. M. Tyrrell, and J. Timmis, "Self-repairing mobile robotic car using astrocyte-neuron networks," in *International Joint Conference on Neural Networks*, 2016, pp. 1379–1386.
[26] G. Perea, R. Gómez, S. Mederos, A. Covelo, J. J. Ballesteros, L. Schlosser, A. Hernández-Vivanco, M. Martín-Fernández, R. Quintana, A. Rayan, A. Díez, M. Fuenzalida, A. Agarwal, D. E. Bergles, B. Bettler, D. Manahan-Vaughan, E. D. Martín, F. Kirchhoff, and A. Araque, "Activity-dependent switch of GABAergic inhibition into glutamatergic excitation in astrocyte-neuron networks," *eLife*, vol. 5, pp. 1–26, 2016.
[27] A. L. Hodgkin and A. F. Huxley, "A quantitative description of membrane current and its application to conduction and excitation in nerve," *The Journal of Physiology*, vol. 117, no. 4, pp. 500–544, 1952.
[28] R. FitzHugh, "Impulses and physiological states in theoretical models of nerve membrane," *Biophysical Journal*, vol. 1, no. 6, pp. 445–466, 1961.
[29] J. Nagumo, S. Arimoto, and S. Yoshizawa, "An active pulse transmission line simulating nerve axon," *Proceedings of the IRE*, vol. 50, no. 10, pp. 2061–2070, 1962.
[30] W. Gerstner and R. Naud, "How good are neuron models?" *Science*, vol. 326, no. 5951, pp. 379–380, 2009.
[31] E. M. Izhikevich, "Simple model of spiking neurons," *IEEE Transactions on Neural Networks*, vol. 14, no. 6, pp. 1569–1572, 2003.
[32] W. Gerstner and W. M. Kistler, *Spiking neuron models: Single neurons, populations, plasticity*. Cambridge University Press, 2002.
[33] Y. Liu and X. Wang, "Spike-frequency adaptation of a generalized Leaky Integrate-and-Fire model neuron," *Journal of Computational Neuroscience*, vol. 10, no. 1, pp. 25–45, 2001.
[34] D. Neil and S.-c. Liu, "Minitaur, an event-driven FPGA-based spiking network accelerator," *IEEE Transactions on Very Large Scale Integration (VLSI) Systems*, vol. 22, no. 12, pp. 2621–2628, 2014.
[35] Q. Yu, R. Yan, H. Tang, K. C. Tan, and H. Li, "A spiking neural network system for robust sequence recognition," *IEEE Transactions on Neural Networks and Learning Systems*, vol. 27, no. 3, pp. 621–635, 2016.
[36] M. Navarrete and A. Araque, "Endocannabinoids potentiate synaptic transmission through stimulation of astrocytes," *Neuron*, vol. 68, no. 1, pp. 113–126, 2010.
[37] J. Hilder, A. Horsfield, A. G. Millard, and J. Timmis, "The Psi Swarm: A low-cost robotics platform and its use in an education setting," in *17th Annual Conference on Towards Autonomous Robotics*, 2016, pp. 158–164.
[38] P. Dempster, J. Harkin, and T. M. Mcginnity, "Tile Implementation Strategy for Self-Repairing Systems," in *IEEE Systems, Man and Cybernetics (SMC) UK&RI Chapter*, 2006, pp. 1–6.

Junxiu Liu received the Ph.D. degree from Ulster University, UK, with the support of a Vice-Chancellors Research Scholarship. His research interests relate to: neural glial system modelling and implementations.

Liam J. McDaid received the B.Eng. (Hons.) degree in Electrical and Electronics Engineering and the Ph.D. degree in solid-state devices from the University of Liverpool, Liverpool, U.K., in 1985 and 1989, respectively. He is currently a Professor of Computational Neuroscience with Ulster University, U.K., and leads the Computational Neuroscience and Neural Engineering Research Team. He has coauthored over 120 publications in his career to date. His current research interests include modeling the role of glial cells in the functional and dysfunctional brain and he is also involved in the development of software/hardware models of neural-based computational systems, with particular emphasis on the mechanisms that underpin self-repair in the human brain. Dr. McDaid received several research grants in this domain and is currently a Collaborator on an HFSP and EPSRC funded project.

Jim Harkin received the B.Tech. degree in electronic engineering, the M.Sc. degree in electronics and signal processing, and the Ph.D. degree from Ulster University, U.K., in 1996, 1997, and 2001, respectively. He is currently a Reader with the School of Computing, Engineering and Intelligent Systems, Ulster University, Derry, U.K. He has authored over 80 articles in peer-reviewed journals and conferences. His current research interests include the design of intelligent embedded systems to support self-repairing capabilities and the hardware/software implementation of spiking neural networks.

Shvan Karim holds a B.Sc. degree in Electrical Engineering from the University of Sulaimani, Kurdistan, Iraq, a M.Sc. degree from the University of Southampton, UK, and is currently a PhD candidate at Ulster University, UK.

Anju P. Johnson is a Post-doctoral Research Associate in the Department of Electronic Engineering of University of York, U.K. since 2016. She received B.Tech degree in Electronics and Communication Engineering from Cochin University of Science and Technology (CUSAT) in the year 2010, M.Tech degree in VLSI Design from Amrita University in 2012 and Ph.D. in Computer Science and Engineering from Indian Institute of Technology (IIT) Kharagpur in the year 2016. Before Joining University of York, she was a Senior Project Officer in the Department of Computer Science and Engineering of IIT Kharagpur (2012-2016) and a faculty (Adhoc) in the Department of Electronics and Communication Engineering, National Institute of Technology (NIT) Calicut (2012). Her research interests include Internet of Things, Hardware Security, Neuromorphic Computing and FPGA Prototyping.

Alan G. Millard received his Ph.D. degree in Computer Science, with a focus on fault detection in swarm robotic systems, from the University of York in 2017. He is currently a research associate in the Department of Electronic Engineering at the University of York, working on the SPANNER project. His current research focus is on engineering fault tolerant swarm robotic systems.

David M. Halliday is a Reader in the Department of Electronic Engineering of University of York the University of York, York, U.K. He received the B.Sc. and Ph.D. degrees in electronics and electrical engineering from the University of Glasgow, Scotland, U.K. He has held research positions at the University of Glasgow, University of Strathclyde, and NTT Basic Research Laboratories, Tokyo. His research interests are in the interdisciplinary fields of Computational Neuroscience and Neural Computing.

Andy M. Tyrrell received a 1st class honours degree in 1982 and a PhD in 1985 (Aston University), both in Electrical and Electronic Engineering. He joined the Department of Electronic Engineering at the University of York in April 1990, he was promoted to the Chair of Digital Electronics in 1998. Previous to that he was a Senior Lecturer at Coventry Polytechnic. Between August 1987 and August 1988 he was visiting research fellow at Ecole Polytechnic Lausanne Switzerland, where he was researching into the evaluation and performance of multiprocessor systems. From September 1973 to September 1979 he worked for STC at Paignton Devon, on the design and development of high frequency devices. He is a Senior member of the IEEE and a Fellow of the IET.

Jon Timmis received the Ph.D. degree in computer science from the University of Wales, Aberystwyth, in 2000, where he also worked as a Research Associate investigating the use of immune system metaphors for machine learning. He is a Professor at the Department of Electronic Engineering, University of York, York, U.K. His primary research interest is in the computational abilities of the immune system and how they relate to computer science and engineering. From 2000 to 2005, he was a Lecturer, then Senior Lecturer at the Computing Laboratory, University of Kent, where he was head of the Applied and Interdisciplinary Informatics (AII) Research Group. Dr. Timmis, in collaboration with Dr. P. Bentley, founded the International Conference on Artificial Immune Systems (ICARIS) in 2002, and is now Chair of the ICARIS Steering Committee. He is on the Editorial Board of Evolutionary Computation (MIT Press).